Electronic Supplementary Material (ESI) for ChemComm.
This journal is © The Royal Society of Chemistry 2018

Electronic Supplementary Information

Porous Ni-O/Ni/Si photoanode for stable and efficient photoelectrochemical water splitting

Guanping Huang, Ronglei Fan, Xiaoxue Zhou, Zihao Xu, Wanyi Zhou, Wen Dong* and Mingrong Shen*

School of Physical Science and Technology, Jiangsu Key Laboratory of Thin Films, Collaborative Innovation Center of Suzhou Nano Science and Technology, Soochow University, Suzhou 215006, China.

* Corresponding Author
E-mail: dongwen@suda.edu.cn

E-mail: mrshen@suda.edu.cn

Experimental section

Materials

Nickel sulfate hexahydrate ($NiSO_4 \bullet 6H_2O$), sodium hydroxide (NaOH) and thiourea were used as received. All reagents were of analytical grade and used without further purification.

The fabrication of pn^+-Si electrodes

Single-crystalline p-Si wafers (1-3 Ω•cm specific resistance, Canadian Solar Inc.) were used for this work. The pyramid surface texture of both sides was produced by a standard process of alkaline etching and then the surface pn^+ junction was fulfilled by a standard process of phosphorus doping. After doping, an anti-reflection SiN_x layer and fritted Ag bar line were produced onto the n^+-Si emitter side. Finally, the samples were laser-cut into 1.5×1.5 cm^2. Before use, Si electrodes were cleaned by subsequent sonication in acetone, ethanol and water for 15 minutes each to remove any contaminants. The native SiO_2 layer on the p-type side was then etched by dropping 5 wt % HF solution. The Si electrodes were then rinsed in deionized water which was degassed by ultrasonic clearing machine (i-Quip, Aladdin) and dried under a stream of N_2.

Magnetron sputtering deposition of Ni films

Ni films were deposited on the textured p-type side by radio frequency (RF) magnetron sputtering (Kurt J Lesker, PVD 75) using a 2 inch Ni target (ZhongNuo Advanced Material, Beijing, China). The base pressure before deposition was less than 5×10^{-7} Pa, and it was kept at 2 Pa using a constant Ar-flow of 30 sccm during the deposition. RF power was 150W with a direct current (DC) bias voltage of 370 V.

Fabrication of photoelectrodes

In order to form an ohmic contact between the copper wire and both sides of Si, tinned Cu wire was embedded in Ag paste and then glued onto the n^+ side (W1, for the photoelectrochemical test) and the Ni surface (W2, for electrochemical measurement and electrodeposition). After the Ag paste is dried completely, a quartz plate (1.5×1.5 cm^2) was adhered to the n^+ surface. At last edges and some part of the front surface of the electrodes (except for the intended reaction area 1×1 cm^2) were sealed with an industrial epoxy (PKM12C-1, Pattex).

Electrodeposition of Ni-S films

The Ni-S film was electrodeposited on the Ni film using the W2 circuit in deposition solution (5 mM $NiSO_4$ and 0.5 M thiourea in water) with Pt sheet as a counter electrode, Ag/AgCl (3M KCl) as a reference electrode. Nitrogen was bubbled through the electrolyte solution for at least 15 min before deposition and maintained during the entire deposition process. The potential of consecutive linear scan was cycled between -1.2 and 0.2 V *vs.* Ag/AgCl at a scan rate of 5 mV/s under stirring. After deposition, the Ni-S/Ni/Si electrode was removed from the deposition bath and rinsed with copious water gently. Finally, Ni-S/Ni/Si was dried under vacuum at room temperature overnight.

Sample characterization

The surface morphology of sample surface was analyzed by field-emission scanning electron microscope (SEM) (SU8010, Hitachi). X-ray photoelectron spectroscopy (XPS) measurements were performed at room temperature using a spectrometer hemispherical analyzer (ESCALAB 250Xi, Thermo). X-ray diffraction (XRD) was measured using an X-ray diffractometer in parallel beam mode with Cu Kα radiation (D/MAX-2000PC, Japanese Rigaku).

PEC and EC measurement

A 300 W Xe lamp (Oriel, Newport Co.) with a silica filter was used as a light source. Before the PEC measurement, the light intensity was carefully controlled at 100 mW/cm^2, measured using an optical power meter (Newport company) just before the light enters into the PEC cell. The measurements were conducted using a solution containing 1 M NaOH with pH=13.6 as electrolyte, the Si photoanode as working electrode, an Ag/AgCl (3M KCl) as reference electrode, and a Pt sheet as counter electrode. The potentials were controlled using an electrochemical workstation (Vertex, Ivium Technologies) and re-scaled to the potential according to the following equation: $V_{RHE} = V_{Ag/AgCl} + 0.197\ V + pH \times 0.059\ V$.

Before the measurement, the Ni-S film was activated through measuring the $J-V$

curves for ten times in 1.0 M NaOH electrolyte, with a Pt sheet as a counter electrode, Ag/AgCl (3M KCl) as a reference electrode, and Ni-S/Ni/Si as a working electrode, under 1 Sun illumination. Then the Ni-S converts into Ni-O.

Polarization curves of Ni-O/Ni/Si were carried out in a solution containing 1 M NaOH in the dark by using the W2 circuit. The IR-drop was not corrected during any of the PEC and EC measurements.

The energy conversion efficiency (η) of the photoanode can be defined as: $\eta = J_m \times (1.23V_{RHE}-V_m) \times \eta_F / P_{in} \times 100\%$. where, J_m and V_m are the photocurrent density (mA/cm^2) and the corresponding calibrated applied bias potential relative to the RHE at the maximum power output, η_F is Faradaic efficiency, and P_{in} is the incident illumination power density (mW/cm^2).

The electrochemical impedance spectroscopy (EIS) curves were obtained at a constant 1.1 V_{RHE} using an electrochemical workstation (Vertex, Ivium Technologies) in the frequency range from 1 Hz to 100 MHz under illumination by W1 circuit.

Electrochemical capacitance was measured using cyclic voltammetry (CV) measurements by W2 circuit in dark. The currents were measured in a narrow potential window that no faradaic processes were observed. CVs were collected at different scan rates: 20, 40, 60, 80, 100, 120, 140, 160, 180 and 200 mV/s. The measured current in this non-faradaic potential region should be mostly due to the charging of the double-layer. The capacitive current was the difference values between two currents at 1.08 V *vs.* RHE.

The hydrogen evolution by PEC water splitting was investigated in an air-tight photo-reactor, which was made of quartz glass. The faradaic efficiency of the illuminated photoanode was determined in a manner similar to the photocurrent measurements at a constant potential of 1.02 V_{RHE} and the amount of H_2 produced was determined using a gas chromatograph equipped with a thermal conductivity detector (Tianmei, GC 7900T). Since our current setup for gas sensing can’t measure the O_2 amount accurately, therefore, O_2 evolution is not presented.

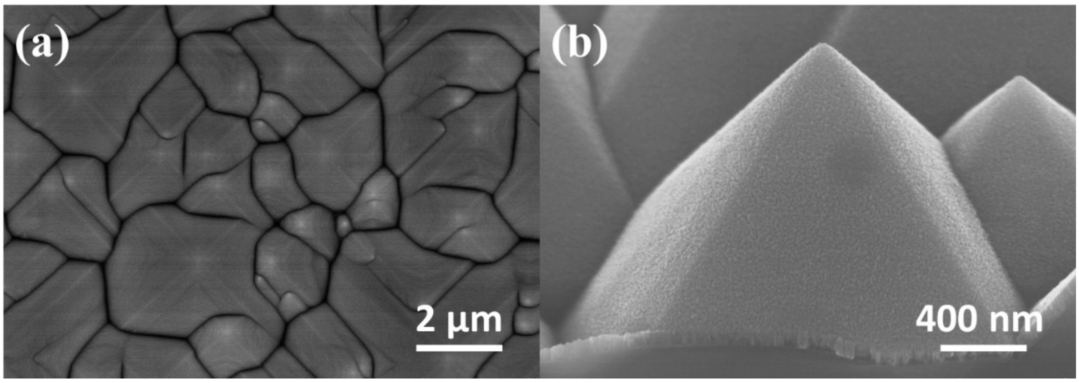

Fig. S1 SEM surface (a) and interface (b) morphologies of Ni/Si sample.

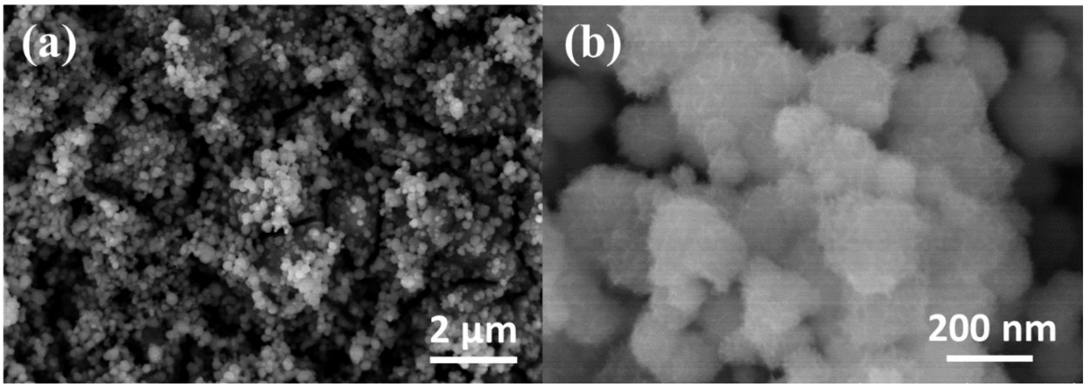

Fig. S2 Surface SEM images of the electrodeposited Ni-S on Ni/Si.

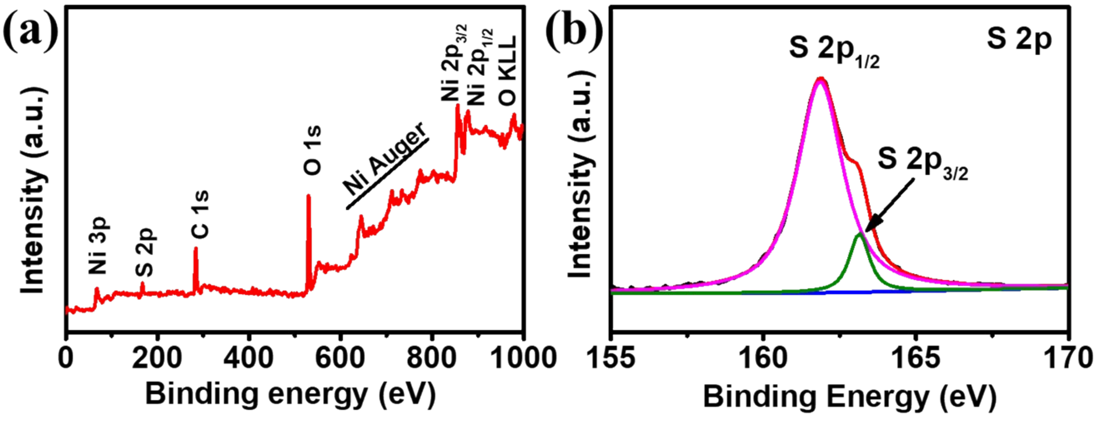

Fig. S3 XPS spectra of as-prepared Ni-S on Ni/Si (a) and high-resolution XPS spectra of S 2p (b).

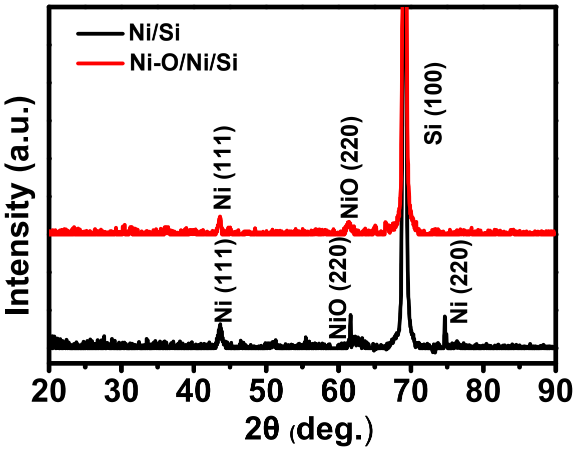

Fig. S4 XRD pattern of Ni/Si and Ni-O/Ni/Si samples.

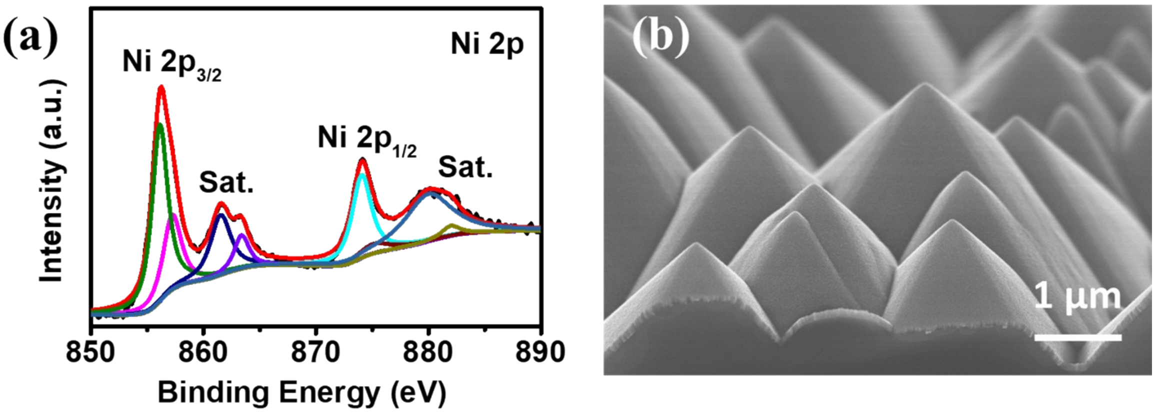

Fig. S5 High-resolution Ni 2p XPS spectra (a) and SEM surface morphology (b) of the dense Ni-O/Ni/Si electrode obtained after the activation of Ni/Si through measuring the *J*−*V* curves for ten times.

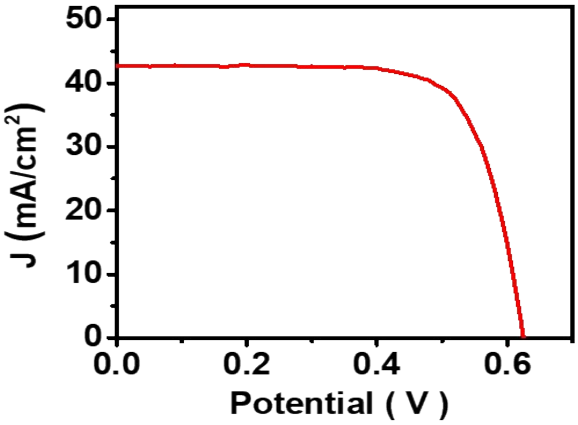

Fig. S6 Current potential (*J*−*V*) characteristics of the solid-state Si solar cells.

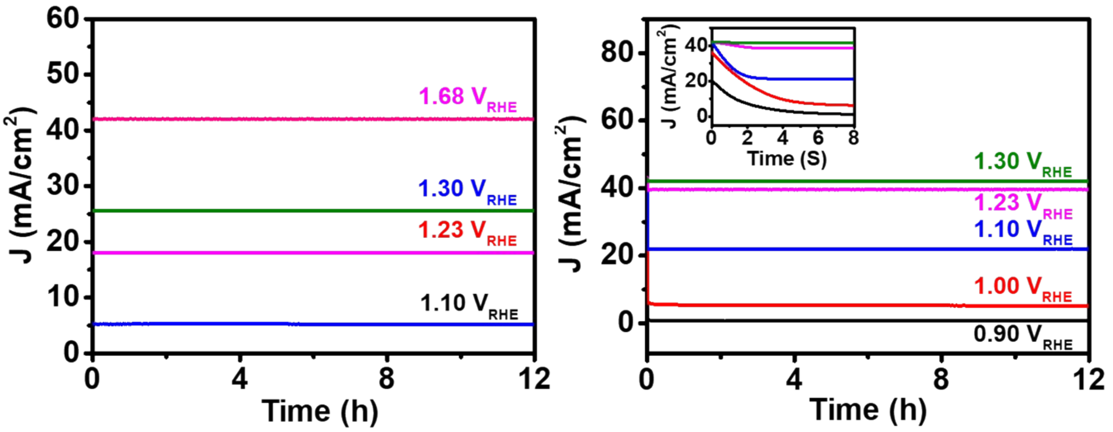

Fig. S7 PEC J-T curves of the dense (a) and porous (b) Ni-O/Ni/Si photoanode with different potentials.

For a true PEC reaction, the obtained photocurrent should be stable. We firstly check the stability of the dense Ni-O/Ni/Si electrode. The photocurrent density at 1.10, 1.23, 1.30, and 1.68 V$_{RHE}$ are all quite stable (Fig. S7a), indicating that the $J-V$ curve is originated from a true PEC reaction. However, we found that the photocurrent for porous Ni-O/Ni/Si is not stable below 1.25 V$_{RHE}$. In Fig. S7b, we present the photocurrent changing with time. When the potential is 1.30 V$_{RHE}$, the photocurrent density is stable. However, it decreases within 8 seconds and then keeps stable when the potential is less than 1.30 V$_{RHE}$. Such decrement within 8 seconds aggravates as the applied potential decreases, and the photocurrent decreases to zero when the potential is lower than 0.90 V$_{RHE}$. Obviously, the left photocurrent after 8 seconds in Fig. S7b is from the true PEC reaction and the decreased current is from the oxidation process of the Ni-O catalyst. From Fig. S7b, we can conclude that the oxidation current under illumination happens within a limited time, therefore we reduce the scan rate of the potential when measuring the photocurrent density, to see the nature of this process.

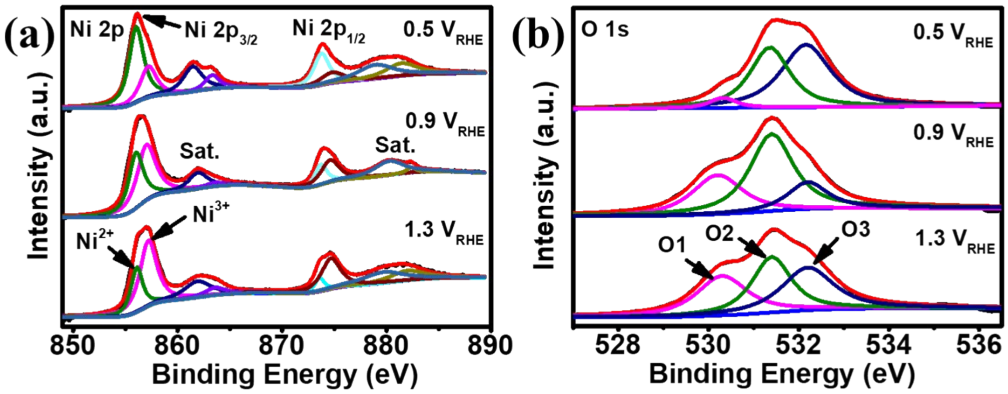

Fig. S8 (a) The Ni 2p and (b) O 1s XPS spectra of the porous Ni-O/Ni/Si photoanode at different disconnected potentials during *J*−*V* measurements.

Photoanode	**V$_{onset}$**	**J$_{1.23}$**	**J$_{sat}$**	**Stability**	**Energy conversion efficiency**	**Irradiation conditions**	**Ref.**
Ni-O/Ni/pn$^+$-Si	0.93	39.7	42	100h 1M NaOH	3.2%	simulated AM 1.5G (1-sun)	Our work
Ni/p$^+$n-Si	1.05	12.7	20.4	240h 1 M KOH	0.47%	simulated AM 1.5G (1-sun)	1
Ni@Ni(OH)$_2$/n-Si	1.03	15.5	36.4	300h K–Bi buffer solution	-	simulated AM 1.5G (1-sun)	2
Ni IO/p$^+$n-Si	0.94	31.2	33	11h 1 M KOH	3.3%	simulated AM 1.5G (1-sun)	3
NiO$_x$/p$^+$n-Si	1.05	29	33	1200 h 1 M KOH	2.1%	simulated AM 1.5G (1-sun)	4
Ni/TiO$_2$/p$^+$n-Si	1	13	33.6	> 100 h 1 M KOH	-	Simulated AM 1.5 G (1-sun)	5

Tab. S1 Comparison of the PEC-OER performance of Si-based photoanodes. V$_{onset}$: onset potential *vs.* RHE (V$_{RHE}$); J$_{1.23}$: photocurrent density at 1.23 V$_{RHE}$ (mA/cm^2); J$_{sat}$: saturation photocurrent density (mA/cm^2).

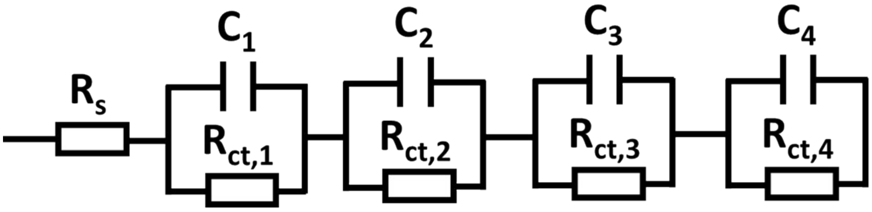

Fig. S9. The equivalent circuits of Ni-O/Ni/Si photoanode. RC1 is the junction in Si, RC2 is the junction on Ni/Si, RC3 is the junction on Ni-O/Ni, and RC4 is the junction on electrolyte/Ni-O.

Photoanodes	$R_{ct,1}$ (Ω)	$R_{ct,2}$ (Ω)	$R_{ct,3}$ (Ω)	$R_{ct,4}$ (Ω)
Dense Ni-O/Ni/Si	3.1	1.0	0.2	20.3
Porous Ni-O/Ni/Si	3.2	0.9	0.3	3.0

Tab. S2 Fitting results for the transfer resistances using the equivalent circuit of Fig. S9.

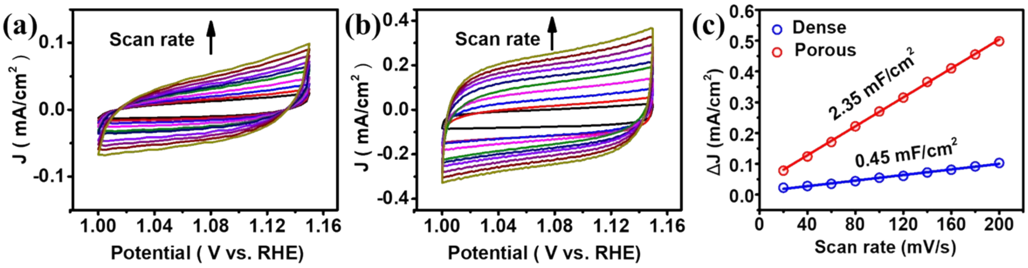

Fig. S10 Cyclic voltammograms of dense (a) and porous (b) Ni-O/Ni/Si photoanodes at different scan rates under dark. (c) Scan rate dependence of the difference of the current densities at 1.08 V_{RHE}.

To estimate the ECSAs of the dense and porous Ni-O surface, the double-layer capacitances (C_{dl}) are evaluated in the CV potential range where no apparent faradaic process occurs. ECSA is proportional to C_{dl} based on ECSA = C_{dl}/C_s, where C_s is the specific capacitance and is considered to be a constant. By plotting the difference in current density between the anodic and cathodic scans ($\Delta j = j_a - j_c$) at a certain overpotential against the scan rate v, a linear relationship could be obtained. The geometric double layer capacitance (C_{dl}) will be enabled by fitting these data to a straight line because $\Delta j = C_{dl} \times v$.[6] The cyclic voltammograms of the dense and porous Ni-O/Ni/Si photoanodes at different scan rates are presented in Fig. S10a-S10b. Then we obtained the plots of Δj changing with the scan rate (Fig. S10c), which show that porous Ni-O/Ni/Si has the much larger C_{dl} (2.35 mF/cm^2) than that of the dense one (0.45 mF/cm^2).

References

1 K. Sun, N. L. Ritzert, J. John, H. Tan, W. G. Hale, J. Jiang, I. Moreno-Hernandez, K. M. Papadantonakis, T. P. Moffat, B. S. Brunschwig and N. S. Lewis, *Sustainable*

Energy Fuels, 2018, **2**, 983.

2 G. Xu, Z. Xu, Z. Shi, L. Pei, S. Yan, Z. Gu and Z. Zou, *ChemSusChem*, 2017, **10**, 2897.

3 S. Oh, H. Song and J. Oh, *Nano Lett.*, 2017, **17**, 5416.

4 K. Sun, M. T. McDowell, A. C. Nielander, S. Hu, M. R. Shaner, F. Yang, B. S. Brunschwig and N. S. Lewis, *J. Phys.Chem. Lett.*, 2015, **6**, 592.

5 S. Hu, M. R. Shaner, J. A. Beardslee, M. Lichterman, B. S. Brunschwig and N. S. Lewis, *Science*, 2014, **344**, 1005.

6 N. Jiang, L. Bogoev, M. Popova, S. Gul, J. Yano and Y. Sun, *J. Mater. Chem. A*, 2014, **2**, 19407.